Heliyon 10 (2024) e39723

Contents lists available at ScienceDirect

Heliyon

journal homepage: www.cell.com/heliyon

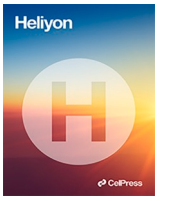

Research article

A low-temperature active and selective bimetallic Cu-In catalysts for hydrogenation of methyl 3-hydroxypropionate to 1,3-propanediol

Chuanming Zhang *, Jincan Kang, Wen Dai, Yanbo Peng, Yiling Zhao, Xiaoang Yang, Bingni Liu, Hongping Zhu **

State Key Laboratory of Physical Chemistry of Solid Surfaces, College of Chemistry and Chemical Engineering, Xiamen University, Xiamen, Fujian, 361005, China

ARTICLE INFO

Keywords:
1,3-Propanediol
Cu catalyst
Cu-In alloy
Low-temperature active
In_2O_3

ABSTRACT

The pathway for producing 1,3-propanediol (1,3-PDO) from methyl 3-hydroxypropionate (3-HPM) has great application potential. However, the reaction is sensitive to temperature and results in reduced product selectivity at high temperatures. This study explores the use of low-temperature active Cu−In bimetallic catalysts for the 3-HPM reaction. The Cu-1In/SiO_2 catalyst exhibits superior catalytic performance with a 91.5 % yield of 1,3-PDO, surpassing that of the Cu/SiO_2 catalyst by 264 % under identical conditions. Multiple characterization methods reveal the textural and physiochemical properties of the catalysts. The excellent catalytic performance of Cu-1In/SiO_2 can be attributed to the introduction of CuIn alloy and highly dispersed In_2O_3. The interaction between copper and Indium species on the catalyst surface facilitates the dispersion of Cu species, while simultaneously highly dispersed In_2O_3 introducing new adsorption sites for reactants, thereby greatly improving its catalytic performance.

1. Introduction

The hydrogenation of Methyl 3-hydroxypropionate (3-HPM) is an important step in the ethylene oxide hydroesterification process for producing 1,3-propanediol (1,3-PDO) [1,2]. The utilization of 3-HPM as an intermediate overcomes the limitations associated with alternative chemical synthesis routes, which are prone to producing unstable intermediate 3-hydroxy propionic aldehyde (3-HPA) [3–5]. However, the hydrogenation of 3-HPM for the synthesis of 1,3-PDO encounter challenges pertaining to reaction selectivity, catalyst efficiency, or reaction conditions. On the one hand, the 3-HPM hydrogenation to 1,3-PDO is a deep hydrogenation reaction that requires harsh conditions and a highly efficiently catalysts carry out the reaction [6]. On the other hand, the side reactions in the hydrogenation process, such as 3-hydroxypropionate, are prone to β-hydroxy dehydration to generate methyl acrylate, deep hydrogenation to produce methyl propionate (MP) and n-propanol (NPA), which are also thermodynamically advantageous [7]. This predisposes the reaction to a trade-off between conversion and selectivity, often referred to as the "teeter-totter" dilemma, where achieving high conversion rates and product selectivity simultaneously is challenging. Generally, in industrial applications, it is highly desirable for catalysts to possess high selectivity towards the desired product. Overly acidic or basic sites within the catalyst can also

* Corresponding author.
** Corresponding author.
E-mail addresses: zhchming163@163.com (C. Zhang), hpzhu@xmu.edu.cn (H. Zhu).

https://doi.org/10.1016/j.heliyon.2024.e39723
Received 3 July 2024; Received in revised form 21 October 2024; Accepted 22 October 2024
Available online 24 October 2024

induce the dehydration and over-hydrogenation of the reactants [6], thus diminishing the selectivity of the catalyst towards the desired product. Therefore, the selection of a neutral catalyst support, such as SiO_2, is crucial for this reaction. And, this imposes a stringent constraint on the reaction temperature, as excessive temperatures can yield unpredictable catalytic outcomes. Therefore, how to prepare a high efficiency catalyst with low temperature activity catalyst to efficiently generate 1,3-PDO target products by hydrogenation of 3-HPM still faces great challenges.

Cu-based catalysts have found extensive applications in hydrogenation of carbon−oxygen bond [8–10], including dimethyl oxalate (DMO), methyl acetate (MA), furfural, CO_2 [11], etc. This performance depends on the synergistic effect of Cu^0 and Cu^+, which activates the C=O bond of H_2, Cu^+ adsorbed ester [12,13]. Due to their exceptional performance and cost-effectiveness in the field of ester hydrogenation, Cu-based catalysts have been chosen as promising candidates for facilitating the synthesis of 1,3-propanediol (1, 3-PDO) through 3-Hydroxypropionate (3-HPM) hydrogenation. However, Cu-based catalyst often suffer from the loss of Cu dispersion due to the severe sintering of Cu nanoparticles under the working condition of the hydrogenation of 3-HPM reaction. More importantly, the Cu-based catalyst exhibited limited catalytic activity at lower reaction temperatures. Thus, the methods to improve hydrogenation of Cu/SiO_2 catalysts attracted much attention.

Metal doping is regarded an effective strategy for modifying and improving the performance of Cu/SiO_2 catalysts in hydrogenation reactions. Cu-based bimetallic catalysts have attracted great attention for the hydrogenation of ester reaction due to their high activity and selectivity. Incorporating trace amounts of noble or transition metals, such as Au [14,15], Ag [16,17], Ni [18,19], Ce [20,21], In Refs. [22,23], and Zn [24,25], onto the Cu/SiO_2 catalyst can effectively modulate its electronic and chemical properties, thereby significantly augmenting its hydrogenation activity. Ding et al. [26] reported that the addition of metal Zn effectively modulated the electrical properties of Cu species, because there was a strong interaction between Zn and Cu, thereby stabilizing Cu^+ species and improving the response ability of Cu^+. Behrens et al. [27] also proved that Zn can effectively stabilize Cu steps on $Cu/ZnO/Al_2O_3$ catalyst by a series of well-defined bulk defects and surface species that need to be present jointly for the system to work. Li et al. [24] found that Zn^{2+}in Ga_2O_3-doped Zn/Cu catalyst can be partially reduced to Zn^0 to form a body-centered cubic (bcc) Cu-Zn alloy, showing high sinter resistance and stability. Wang et al. [28] also found that appropriate Zn incorporation could improve the Cu^+ content on the catalyst surface and the dispersion of Cu^0 particles, and make the catalyst have better sintering resistance. However, the performance of these catalysts for ester hydrogenation at low temperature remains to be investigated.

Recently, indium oxide (In_2O_3) has been reported as a highly selective and stable catalyst for methanol synthesis from CO_2 [29–31]. However, the weakness of In_2O_3 in H_2 dissociation limits its activity for CO_2 hydrogenation [32–34]. In this context, the design of Cu−In bimetallic catalysts can achieve two different goals in a single action, as the dispersion of Cu can be improved by introducing a defective oxide (i.e., In_2O_3) and the H_2 dissociation ability of In_2O_3 can be enhanced by Cu [35]. The catalyst design was quickly applied to the ester hydrogenation reaction and exhibited good catalytic activity [22,23]. Zhang et al. [22] reported on the application of indium oxide-modified Cu/SiO_2 catalysts in the methanolysis of methyl acetate for the preparation of ethanol. The study suggests that the appropriate introduction of indium increases the dispersion of copper in the catalyst, reduces the copper grain size, and increases the surface copper concentration. Ma et al. [23] reported that the plentiful interface of Cu^+–CuIn alloy prompts the conversion of the carbonyl group adsorbed on the Cu^+ sites with the dissociated hydrogen on the vicinal CuIn alloy. Despite extensive studies, some mechanistic insights remain elusive for Cu−In bimetallic catalysts in hydrogenation [36–39]. Yu et al. [40] argue that the presence of indium species has a negligible effect on the content of Cu^+ species on the surface. Instead, they suggest that the promotional effect likely arises from interactions between reduced indium species and Cu^0 species, which enhances the latter's ability to activate H_2. Bossola et al. [41] reported that the formation of InO_x "necklace" buffer phases at the interface between the Cu nanoparticles and the silica support in Cu-In/SiO_2 catalyst, thus an enrichment of electron density of the Cu nanoparticles. The promotional effect of the In component on the copper-based catalyst remains elusive. The hydrogenation of 3-HPM reaction requires higher pressure but lower temperature compared to DMO-to-EG, making it attractive to investigate the catalytic performance and active phase of Cu−In bimetallic catalysts under such conditions.

On this basis, a series of Cu-*x*In/SiO_2 catalysts with different contents of In modification were prepared by distilled ammonia method in this study. And a series of characterizations such as H_2-programmed temperature reduction (H_2-TPR),X-ray diffraction (XRD), transmission electron microscopy (TEM), and X-ray photoelectron spectroscopy (XPS) were carried out to deeply explore the promotion effect of indium on Cu/SiO_2 and to further study the correlation between the structure and its performance.

2. Experimental

2.1. Materials

$Cu(NO_3)_2{\cdot}3H_2O$, $In(NO_3)_3{\cdot}3H_2O$, ethanol, aqueous ammonia solution ($NH_3{\cdot}H_2O$, 28 wt%), and methanol purchased from Sinopharm Chemical Reagent Co., Ltd. Silica sol (mass fraction of SiO_2 is 30 %) purchased from Qingdao Ocean Chemical Co., Ltd. These reagents and chemicals were analytically pure (AR) and used without further purification. Methyl 3-hydroxypropionate (3-HPM) was prepared in our lab by the patent method [42].

2.2. Catalyst preparation

The Cu-*x*In/SiO_2 catalysts (*x* denotes the nominal indium mass loading) was prepared by the ethanol-assisted ammonia evaporation method (Et-AE). All catalysts contained a constant, pre-set Cu loading of 20 wt %. An aqueous ammonia solution (28 wt%) was initially mixed with a calculated amount of $Cu(NO_3)_2{\cdot}3H_2O$ and $In(NO_3)_3{\cdot}3H_2O$ aqueous solution (300 mL water and 150 mL ethanol) under

vigorous stirring for 30 min. Subsequently, a calculated amount of silica sol (SiO_2, 30 wt%) was dropped into the above copper ammonia complex solution through the peristaltic pump and stirred for 30 min at room temperature. Subsequently, the suspension was further stirred under 363 K in a water bath to evaporate ammonia and deposit copper species on silica. The evaporation process was terminated when the pH of the mixture declined from 11 to 12 to 6–7. The precipitate was filtered, washed with deionized water, dried overnight at 393 K (marked as Cu-*x*In/SiO_2 precursors). And then the catalyst precursor was calcined at 723 K (10 K/min) for 240 min, followed by calcining at 923 K (1 K/min) for 300 min. And then the Cu-*x*In/SiO_2 ($x = 0$, 0.25, 0.50, 1.0 and 2.0 wt%) catalysts were obtained, where x represents the weight ratio of In. For comparison, 2%In/SiO_2 (2.0 wt%) catalyst was prepared by the same preparation method.

2.3. Characterization

N_2 adsorption-desorption isotherms were measured at 77 K using a Micromeritics ASAP 2020C instrument after degassing at 523 K for 3 h to remove physically adsorbed impurities. The relative pressure (P/P_0) was varied from 0.01 to 1.0 to obtain the texture structure parameters of the catalyst. The specific surface area was calculated by the Brunauer-Emmett-Teller (BET) method. The Barrett-Joyner- Halenda (BJH) method was applied to calculate the pore size distributions according to the desorption branches of the isotherms.

Loadings of either Cu or In metal or both in the catalysts were determined by the inductively coupled plasma-optical emission spectrometer (ICP-OES, Agilent 5110, USA). Samples were prepared by dissolving in HF followed with addition of H_3BO_3 aqueous solution.

Fourier transform infrared (FT−IR) spectroscopy was recorded on a Nicolet iS50 spectrometer (USA) with a spectral resolution of 4 cm^{-1}. The wave number range was from 4000 to 400 cm^{-1}, and 32 scans were recorded for each spectrum.

Wide-angle X-ray diffraction (XRD) scanning was conducted on a Rigaku Ultima-IV X-ray diffractometer equipped with Cu K_α radiation at 40 mA and 40 kV. The data were recorded from 2θ of 10–90° with a continuous scanning speed of 20°/min. The mean crystallite sizes of the CuO and Cu supported were calculated with the Scherrer equation.

The reducibility of the calcined sample was determined by H_2 temperature-programmed reduction (H_2-TPR) on a multifunctional catalyst characterization instrument (MTP3060, Betterwork, China). Calcined catalyst sample (100 mg) in a quartz U-tube reactor was pre-treated at 423 K for 1 h under a 30 mL/min flow of Ar. After being cooled to room temperature under an argon atmosphere, a 5 % H_2/Ar was introduced at a flow rate of 30 mL/min. Subsequently, the temperature was linearly increased from ambient temperature to 893 K at a rate of 10 K/min, and the amount of consumption H_2 was measured by a TCD detector.

Copper dispersion is a vital index related to catalytic performance. N_2O titration experiment was performed on a multifunctional catalyst characterization instrument (MTP3060, Betterwork) apparatus to determine the copper dispersion according to a literature procedure [43].

Temperature-programmed desorption (TPD) was performed with Micromeritics Autochem II ASAP 3060 instrument. Firstly, the catalyst was allowed to adsorb the reactant 3-HPM in the reaction apparatus. The specific steps are as follows: The catalyst was activated for 2 h at 578 K (1 K/min) using an argon gas stream containing 5 % hydrogen (90 mL/min). After cooling to 433 K, the gas stream was switched to pure hydrogen (99.99 %). The liquid 3-HPM was then introduced into the reactor by bubbling with hydrogen. This process continued for 1.5 h, after which the injection of 3-HPM liquid was stopped, and the reactor was further purged with hydrogen for an additional 0.5 h at the same temperature. The system was then cooled to room temperature, and the catalyst was inerted using a gas stream of 1 % O_2/Ar, ready for use. The catalyst sample (100 mg) completed 3-HPM adsorption in a quartz U-tube reactor was pre-treated at 373 K for 1 h under a 30 mL/min flow of Ar. Then the sample was heated to 1073 K in Ar flow. The quantity of desorbed products was detected by TCD and MS signal.

X-ray photoelectron spectroscopy (XPS) and X-ray Auger electron spectroscopy (XAES) were measured on a Quantum 2000 Scanning ESCA Microprobe instrument (Physical Electronics produced by PHI) equipped with an Al K_α X-ray radiation source (E = 1486.6 eV). The Cu 2p spectral region of the sample was recorded, where the carbonaceous C 1s line (284.6 eV) was used as the reference to calibrate the bonding energies (BEs). The calcined catalyst sample was heated to 578 K in 5 % H_2/Ar at 30 mL/min and reduced at this temperature for 1 h. After reduction, the sample was kept under Ar and transferred into the XPS chamber for test when cooling to room temperature.

Transmission electron microscopy (TEM) was measured on a Philips FEI Tecnai 20 electron microscope with an operating voltage of 200 kV. The catalyst is pre-reduced and inerted with 1%O_2/Ar gas prior to testing. The sample was milled and ultrasonically dispersed in ethanol at room temperature for 15 min and then deposited on copper grid coated with amorphous film.

2.4. Catalytic performances

Catalytic performances Catalytic evaluation of 3-HPM hydrogenation to 1,3-PDO with a stainless-steel fixed-bed tubular reactor (inner diameter of 8 mm and length of 650 mm). 1 g of catalyst (40–60 meshes) was packed in the tubular reactor at a zone with constant temperature. The catalyst was activated in a flow of H_2/Ar (5 %/95 %) atmosphere (90 mL/min) at 423 K for 30 min with a ramping rate of 10 K/min, then at 573 K for 2 h with a ramping rate of 1 K/min. The reactor was cooled to the target reaction temperature 433 K, and H_2 was fed into the reactor using a mass flow controller. The system pressure was precisely controlled at 6 MPa with a back-pressure regulator. After reduction, a 10 wt% 3-HPM methanol solution was continuously pumped into the reactor with a micro-pump along with co-feeding H_2 of gas flowing at 220 cm^3 min^{-1}. Reaction conditions: T = 433 K, P(H_2) = 6.0 MPa, WHSV(3-HPM) = 0.1 h^{-1}, H_2/3-HPM = 240. The products were condensed and analyzed by the gas chromatography (GC2060, Shanghai

Keenan Company) fitted with an OV-1701 column (30 m × 0.53 mm) and a flame ionization detector. The effluents mainly include the un-converted 3-HPM, 1,3-PDO, methyl propionate (MP) and n-propanol (NPA). The calculation of the conversion of 3-HPM and selectivity to various products (1,3-PDO, MP and NPA) follows formula below:

$$X_{HPM} = \left(1 - \frac{n_{HPM,out}}{n_{HPM,in}}\right) \times 100\% \quad (1)$$

where $n_{MHP,out}$ and $n_{MHP,in}$ are the amount of HPM (mole) in products and feed reactants, respectively.

$$S_{PDO} = \frac{n_{PDO}}{n_{HPM,in} - n_{HPM,out}} \times 100\% \quad (2)$$

$$S_{MP} = \frac{n_{MP}}{n_{HPM,in} - n_{HPM,out}} \times 100\% \quad (3)$$

$$S_{NPA} = \frac{n_{NPA}}{n_{HPM,in} - n_{HPM,out}} \times 100\% \quad (4)$$

where n_{PDO}, n_{NPA} and n_{MP} are the amount of 3-HPM (mole) converted for the formation of product 1,3-PDO, MP and NPA (mole), respectively.

3. Results and discussion

3.1. Catalytic performance

The properties of a series of Cu-*x*In/SiO_2 samples (x = 0, 0.25, 0.50, 1.0 and 2.0 wt%) were evaluated using the 3-HPM hydrogenation reaction, and the corresponding results are presented in Table 1 and Fig. 1. The results demonstrate that at 433 K and 6 MPa, with a WHSV(3-HPM) of 0.15 h^{-1} and H_2/3-HPM ratio of 240, the conversion of 3-HPM initially increases as the In loading increases, but subsequently decreases upon reaching a load of 2%In. The selectivity trend exhibited an inverse relationship with the conversion trend, and the predominant by-product was NPA, which resulted from further hydrogenation of 1,3-PDO. It is noteworthy that, in contrast to the reaction results obtained under conditions at 433K (Table 1), all catalysts maintained over 90 % selectivity towards 1,3-PDO under the reaction conditions at 413K (Fig. 1), as anticipated. This suggests that lower reaction temperatures confer an advantage for enhancing the product selectivity of the catalysts. The variations in catalytic performance resulting from changes in the indium content in the catalyst can be attributed to characteristics such as Cu particle size and Cu^+ charge intensity. Furthermore, the Cu-1In/SiO_2 samples exhibited superior catalytic activity and yielded the highest amount of 1,3-PDO under the given reaction conditions. The stability testing of the Cu-1In/SiO_2 catalyst was conducted under conditions of high conversion rate, considering the intricate relationship between conversion rate and selectivity.

Various characterization methods have been conducted to reveal the catalytic behavior of the Cu-based catalysts for 3-HMP hydrogenation, and the results are discussed as follows.

3.2. Catalyst morphology and Crystalline phase

The outcomes of the inductively coupled plasma-optical emission spectrometer (ICP-OES) analyses for the calcined Cu-*x*In/SiO_2 catalyst series (x = 0, 0.25, 0.50, 1.0, and 2.0 wt%) following calcination are presented in Table 2. The actual loadings of copper and indium on the catalysts slightly exceed the theoretical values, yet this variance is negligible. ICP-OES display the actual metal loadings are close to the theoretical values, proves the effectiveness of the preparation method which can deposit most of the copper and indium species onto the silica support.

The chemical compositions and textural properties of all catalysts are summarized in Table 2. The N_2 physisorption measurement shows that all the calcined samples exhibit similar type IV isotherms and H1-type hysteresis loops [44], which are usually given by mesoporous adsorbents (Fig. S1a). The pore volume and the pore size for these Cu-*x*In/SiO_2 catalysts rises from 0.54 to 0.65 cm^3/g and 0.74–0.83 nm with their different indium loading dosages from 0 to 1 wt%. The of samples with low indium loading amount (0–1 wt%) was almost unchanged. However, the samples containing 2 wt% of indium species exhibit a reduction in S_{BET} by 13.1 % compared to

Table 1
Effect of the loading amount of In on the catalytic hydrogenation of 3-HPM to 1,3-PDO.

Catalysts	Conversion of 3-HPM (%)	Selectivity to 1,3-PDO (%)	Selectivity to MP (%)	Selectivity to NPA (%)	Yield of 1,3-PDO (%)
Cu/SiO_2	61.3	85.4	11.2	3.4	52.4
Cu-0.25In/SiO_2	92.1	84.5	4.9	10.6	77.8
Cu-0.5In/SiO_2	96.7	81.7	4.9	13.4	79.0
Cu-1In/SiO_2	99.8	75.3	2.3	22.4	75.1
Cu-2In/SiO_2	60.9	91.0	3.9	5.1	55.4

Reaction conditions: T = 433 K, P(H_2) = 6.0 MPa, WHSV(3-HPM) = 0.15 h^{-1}, H_2/3-HPM = 240.

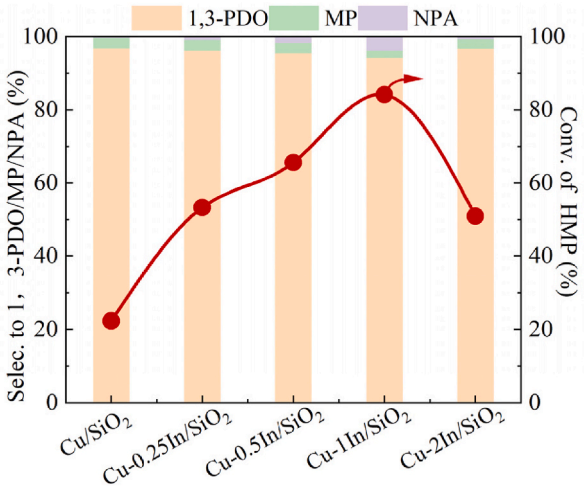

Fig. 1. Activity tests of Cu-*x*In/SiO_2 catalysts (x = 0, 0.25, 0.50, 1.0 and 2.0 wt%). Reaction conditions: T = 413 K, P(H_2) = 6.0 MPa, WHSV(3-HMP) = 0.15 h^{-1}, H_2/3-HPM = 240.

Table 2
Physicochemical characterization of catalysts loaded with different amounts of indium.

Catalysts	Cu content (wt %)[a]	In content (wt %)[a]	S_{BET}[b] (m^2/g)	*V*pore[c] (cm^3/g)	*D*pore[d] (nm)	Cu Particle size (nm) e	Cu Particle size (nm)[f]
Cu/SiO_2	20.8	–	293.5	0.54	7.4	8.6	5.7
Cu-0.25In/SiO_2	20.3	0.26	301.7	0.61	8.1	–	3.3
Cu-0.5In/SiO_2	20.2	0.53	303.9	0.64	8.3	–	3.7
Cu-1In/SiO_2	20.4	1.01	306.1	0.65	8.3	–	2.6
Cu-2In/SiO_2	20.1	2.04	266.3	0.51	7.7	12.7	7.1

Note.
[a] Determined by ICP-OES analysis.
[b] Specific surface area.
[c] Pore volume.
[d] Pore diameter, P/P_0 = 0.995.
[e] Calculated from XRD.
[f] Obtained through TEM measurement.

the Cu-1In/SiO_2 catalyst. Both pore volume and pore size decrease, potentially attributed to pore blockage caused by high loading of indium oxide particles. Additionally, the unique structure of copper phyllosilicate (CuPS) [45] provides a significant S_{BET}. The incorporation of a high indium loading in Cu-Si-based catalysts may potentially impede the interaction between copper and silicon [6], thereby hindering the formation of CuPS. This could also plausibly account for the alteration observed in the Cu-2In/SiO_2 catalyst's pore structure.

It is noteworthy that while the variation in S_{BET} of Cu-*x*In/SiO_2 catalysts (x = 0, 0.25, 0.50, 1.0, and 2.0 wt%) aligns with the trend of catalyst activity, a significant enhancement in catalytic performance within the range of (x = 0, 0.25, 0.50, and 1.0 wt%) appears to be independent of the marginal increase in catalyst S_{BET}. While previous studies [46,47] have successfully enhanced the catalytic performance and stability of similar ester hydrogenation reactions through increased surface area, this study faced challenges in demonstrating the significant role of augmented catalyst surface area and pore volume in the 3-HPM hydrogenation process. The decline in specific surface area and pore volume is likely a crucial factor contributing to the decreased catalytic performance of the Cu-2In/SiO_2 catalyst. Moreover, the presence of the peaks at 3 nm for all the catalysts (Fig. S1b) proves the existence of copper phyllosilicate which can be reduced to Cu^+ species [46]. In addition, it has been reported that copper species like copper phyllosilicate in the catalysts may promote the ester hydrogenation processes (such as DMO and diethyl malonate (DEM)) [48,49]. Therefore, the copper species involved in the hydrogenation of 3-HPM were investigated in this study.

FT-IR characterization was utilized to reveal structural information for the Cu-*x*In/SiO_2 precursors samples shown in Fig. 2a, which is a useful technique for distinguishing copper phyllosilicate phase. FT-IR spectra confirm the presence of $Cu_2Si_2O_5(OH)_2$ (copper phyllosilicate) in Cu-*x*In/SiO_2 (x = 0, 0.25, 0.50, 1.0 and 2.0 wt%) precursors as evidenced by deformation band (δ_{OH}) of OH at 670 cm^{-1} and asymmetric stretching vibration band (ν_{SiO}) of Si–O at 1040 cm^{-1} [50]. The bands at 1117 and 803 cm^{-1} ascribed to asymmetric stretching vibration band (ν_{SiO}) and the symmetric stretching vibration band (ν_{SiO}) in the amorphous silica. The relative content of copper phyllosilicate in each sample can be estimated using I_{670}/I_{800} [51]. The I_{670}/I_{800} ratios of Cu-*x*In/SiO_2 precursors

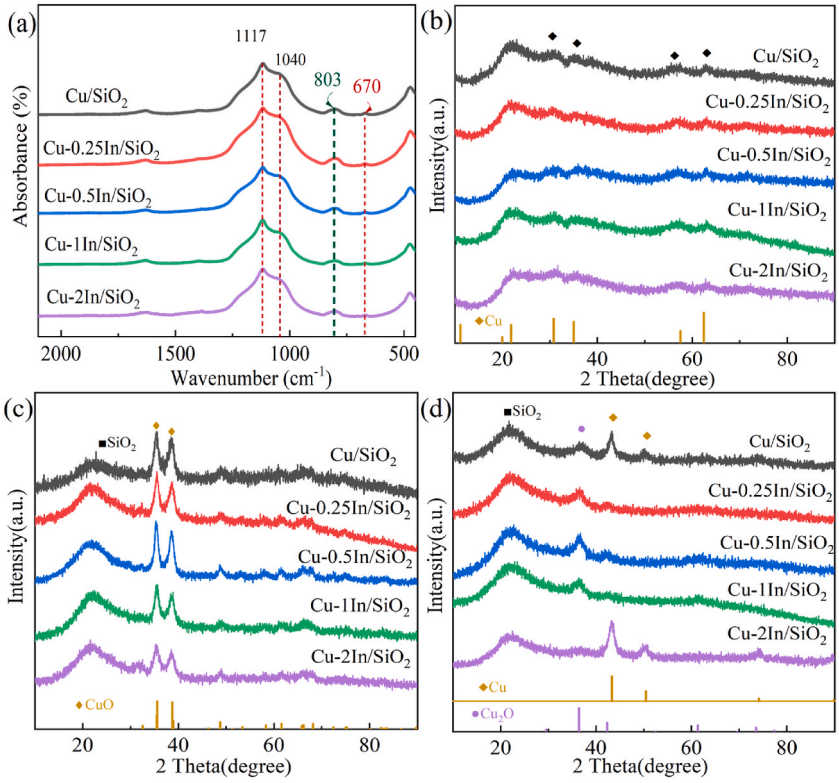

Fig. 2. (a) FT-IR spectra of the Cu-*x*In/SiO_2 precursors; (b) XRD spectrum of Cu-*x*In/SiO_2 precursors; (c) XRD spectrum of calcined Cu-*x*In/SiO_2; (d) XRD spectrum of reduced Cu-*x*In/SiO_2.

undergo marginal alterations across various indium loading doses ranging from 0 to 2 wt% (Table S1), exhibiting a parallel trend with the variations observed in S_{BET}. However, the I_{670}/I_{800} ratio merely offers a qualitative assessment of the copper phyllosilicate content, as the extinction coefficients for the respective IR bands remain unknown. Therefore, discussions concerning the variation in CuPS content within the catalyst must be approached with greater caution. Moreover, the XRD patterns of the Cu-*x*In/SiO_2 precursors (Fig. 2b) further corroborate the presence of copper phyllosilicate within the catalyst precursor. The weak peaks observed at $2\theta = 30.8°$ and 35.0° correspond to the characteristic peaks of $Cu_2Si_2O_5(OH)_2$ (JCPDS41-1390). Obviously, copper phyllosilicate exists in all the catalyst samples, which shows poor crystallinity as other researchers have reported [46,52].

In order to investigate the impact of introducing In on the Cu/SiO_2 catalyst, X-ray diffraction (XRD) patterns were obtained for both the calcined samples and reduced catalysts of the Cu-*x*In/SiO_2 catalyst, as depicted in Fig. 2c and d. All samples exhibit diffraction lines attributed to the silica support, displayed a single broad peak centered at 2θ of 23°, which was characteristic of amorphous silica. The XRD patterns of calcined samples (Fig. 2c) exhibit relative broad diffraction peaks at 35.4° and 38.6°correspond to CuO (002) and CuO (111) (JCPDS 05–0661) implying CuO does not undergo severe agglomeration even after 923 K calcined treatment in Cu/SiO_2 and Cu-*x*In/SiO_2.

After reduction (Fig. 2d), Cu/SiO_2 show a strong diffraction peak at $2 = 43.3°$ along with three weak ones at 50.4°, 74.1° and 85.0° characteristic of Cu^0 (JCPDS04-0836), and a weak and broad peak at around 36.4° ascribable to the Cu_2O (111) (JCPDS05-0667) plane can also be observed, indicating that at least Cu_2O and Cu^0 are present in Cu/SiO_2. The sharper Cu diffraction peaks stem from a certain degree of agglomeration occurring during the reduction process of the catalyst. Meanwhile, the broader Cu_2O diffraction peaks originate from the highly dispersed copper phyllosilicate reduction, further corroborating the assessments of the presence of copper phyllosilicate by FT-IR and BET. The Cu-0.25In/SiO_2, Cu-0.5In/SiO_2, and Cu-1In/SiO_2 catalysts exhibit diffraction peaks resembling those observed for the Cu/SiO_2 catalyst, with a similar pattern of Cu_2O peaks but notably diminished Cu peaks. This reduction in intensity is particularly pronounced for the Cu-1In/SiO_2 catalyst, suggesting that the introduction of an appropriate amount of In assists in suppressing the agglomeration of Cu during the reduction process. This effect can potentially be attributed to the strong interaction between In_2O_3 and Cu during reduction. The high dispersion of Cu^0 facilitates the activation and deionization of hydrogen, thereby positively influencing the catalyst's activity. This is highly effective in enhancing catalytic activity. For the Cu-2In/SiO_2 catalyst, there are smaller Cu_2O diffraction peaks and more pronounced Cu diffraction peaks, indicating that the excessive introduction of In disrupts the formation of copper phyllosilicate in the catalyst, while also exerting a negative impact on the dispersion of Cu. Additionally, the XRD patterns of all catalysts after reduction showed no discernible diffraction peaks attributed to CuO, indicating its absence. Based on the H_2-TPR test and XPS analysis of the reduced catalyst, it can be inferred that all Cu^{2+} species within the catalyst were completely reduced to metallic Cu^0 and Cu^+ ions under the given reduction conditions. Additionally, the XRD pattern of the Cu-

In/SiO_2 catalyst shows no distinct diffraction peaks for In_2O_3 or In^0, which may indicate that the indium in the catalyst is highly dispersed, or it could be due to the low content of indium, possibly below the detection limit of XRD.

The catalyst activated by H_2 reduction at 578 K was characterized using TEM (Fig. 3) to gain deeper insights into the particle distribution and crystal phase within the catalyst. It can be seen that the light-gray SiO_2 carrier on the surface is densely covered by black metal nanoparticles [53]. The average particle size data of the catalyst was obtained through statistical analysis in the atlas. the particle size of Cu species in the catalyst showed the following trends: Cu-1In/SiO_2 < Cu-0.25In/SiO_2 < Cu-0.5In/SiO_2 < Cu/SiO_2 < Cu-2In/SiO_2. The observed trend aligns with the pattern exhibited by the particle size of Cu species in XRD statistics (Fig. 2d) and the dispersion behavior of Cu in N_2O titration experiments (Table S2). The Cu nanoparticles in the Cu-*x*In/SiO_2 ($x = 0.25, 0.5, 1$) catalyst are well dispersed on the support. And the average particle size of Cu nanoparticles in the reduced Cu-1In/SiO_2 catalysts is significantly smaller than that in the Cu/SiO_2 catalyst without indium introduction, as indicated by statistical analysis in the atlas and confirmed by XRD data suggests that the interaction between copper and indium effectively prevents Cu agglomeration during reduction. Additionally, high-resolution electron microscopy of Cu/SiO_2 revealed simultaneous observation of Cu (200) and Cu_2O (200), providing

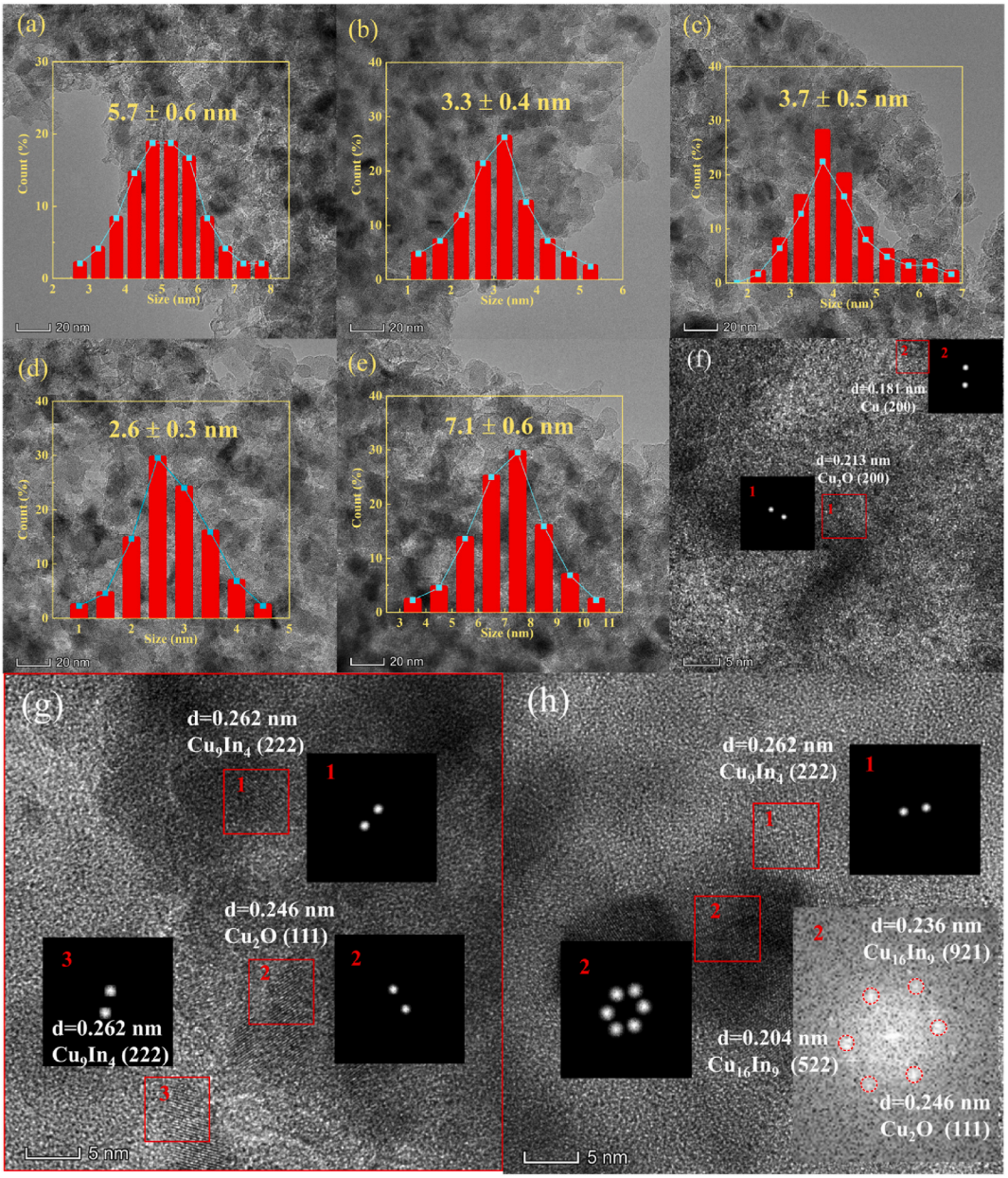

Fig. 3. TEM images of reduced catalysts: (a)Cu/SiO_2, (b)Cu-0.25In/SiO_2, (c)Cu-0.5In/SiO_2, (d)Cu-1In/SiO_2, (e)Cu-2In/SiO_2 and HRTEM image of (f)Cu/SiO_2, (g)Cu-1In/SiO_2, (h)Cu-2In/SiO_2.

further support for the coexistence of Cu^0 and Cu^+ in catalyst (Fig. 3f). The crystal phase of Cu_9In_4 (222) and $Cu_{16}In_9$ (111) (522) (921) were observed in high-resolution electron microscopy of the Cu-In/SiO_2 catalyst (Fig. 3g and h), indicating that the interaction between In and Cu promotes the reduction of In_2O_3 and forms a CuIn alloy. Similar results have been found in related studies [23,36,38], but the difference lies in the fact that previous studies mostly focused on alloys containing $Cu_{11}In_9$, whereas the variation in alloy types observed here may be attributed to the higher roasting temperature used. Cu electronic structure is modulated with the formation of a CuIn alloy which improves the adsorption intensity for H_2 [54], which may promote the high activity of Cu-In/SiO_2 catalyst in the ester hydrogenation reaction. And the formation of a CuIn alloy was observed to further enhance the stability of Cu nanoparticles and maintain their highly dispersed state on thereby positively contributing to the catalyst's overall stability.

3.3. Chemical states of surface species

To further corroborate the crystal phase mutation during reduction activation, H_2-TPR was conducted to qualitatively depict the reducibility of the copper-based catalysts and 2In/SiO_2 (Fig. 4a). The Cu-*x*In/SiO_2 ($x = 0$, 0.25, 0.50, 1.0 and 2.0 wt%) catalysts exhibit asymmetric reduction peaks at temperatures ranging ca. 450 K–570 K, which can be attributed to the overlapping of two sets of reduction peaks corresponding to the transformation of copper silicate into Cu^+ and CuO crystal into Cu^0, respectively [9,55,56]. It is evident that the introduction of indium component leads to a significant increase in the main reduction temperature of the catalyst, primarily attributed to the interaction between copper and indium during the reduction process, rendering it more challenging for CuO crystals to undergo reduction to Cu^0. Additionally, TPR characterization revealed that the reduction peak of the Cu/SiO_2 catalyst exhibited pronounced asymmetry, whereas the Cu-In/SiO_2 catalyst displayed a reduction peak with improved symmetry. Corroborated by XRD and TEM analyses, it is inferred that this transformation is primarily attributed to the addition of indium, which enhances the dispersion of copper on the silicon support. The more homogeneous distribution of copper leads to smaller particle sizes and a more uniform reduction process, thereby resulting in a symmetrical reduction peak. The reduction shoulder peaks observed in the temperature range of ca. 570–800 K can be attributed to the overlapping reduction peaks of larger CuO particles and highly dispersed In_2O_3 [23]. It is noteworthy that the reduction temperature of In_2O_3 in Cu-*x*In/SiO_2 is notably lower than that in 2In/SiO_2 (ca. 922.3 K). This is due to the interaction between Cu species and In species, which favors the formation of highly dispersed In_2O_3 species, thereby promoting the reduction of In_2O_3. Consequently, this increases the likelihood of alloy formation in the catalyst at activation temperatures (578 K). Furthermore, subsequent In *3d*-XPS analysis confirmed partial reduction of In_2O_3 in the Cu-*x*In/SiO_2 catalyst.

The XPS and XAES spectrogram were used to evaluate the valence states for surface copper species. In the XPS spectra of the Cu/SiO_2 catalysts reduced at 578 K (Fig. 4b), the peaks at 933.0 eV and 953.0 eV are assigned to Cu *2p 3/2* and Cu *2p 1/2* respectively. In the XPS spectra of Cu/SiO_2 and Cu-*x*In/SiO_2 catalysts, the peak centered around 932.7–933.1 eV corresponds to the Cu *2p3/2* peak, with a shoulder peak observed at higher binding energies. There are almost no significant Cu^{2+} photoelectron peaks observed between 940–945 eV, indicating that the majority of Cu^{2+} on the surface can be reduced to Cu^0 and/or Cu^+ [57]. Furthermore, compared to the XPS spectra of the Cu/SiO_2 catalyst, with the introduction of In into the Cu-*x*In/SiO_2 catalyst, a gradual shift of the Cu *2p* peak towards lower binding energies is observed. The red shift of the Cu *2p* peak in the catalyst may be attributed to an increase in the surface electron cloud density of copper species [58], indicating a strong interaction between copper and indium species, leading to surface charge transfer between the two metals species.

In the hydrogenation reaction of relevant esters, thorough investigation into both oxidation states of copper is imperative due to the distinct catalytic roles attributed to Cu^0 and Cu^+ [6,59]. Since XPS cannot accurately distinguish between Cu^0 and Cu^+, Cu LMM XAES was recorded to discriminate these peaks [60,61]. The presence of auger kinetic energy peaks ranging from 907.0 to 922.0 eV suggests co-existence of the active Cu^+ and Cu^0 sites (Fig. S2). The original spectra obtained from the catalysts at 907.0–922.0 eV are deconvoluted into two peaks: one at approximately 914.4 eV is attributed to Cu^+, and the other at around 917.6 eV is ascribed to Cu^0 [62,63]. The Cu^+ species plays a crucial role in the adsorption of the ester group from the reactant. Notably, an increased $Cu^+/(Cu^0+Cu^+)$ ratio results in enhanced adsorption of the ester group, thereby corresponding to heightened catalytic activity of the catalyst. The peak integration calculations presented in Table 3 reveal that as the indium content in the Cu-*x*In/SiO_2 catalysts (0–2 wt%)

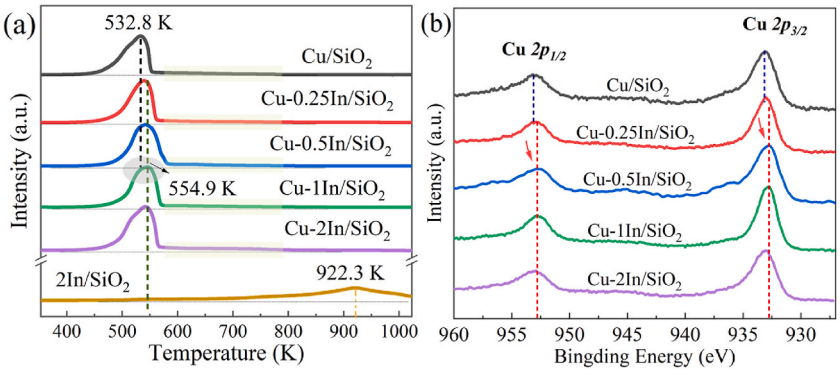

Fig. 4. (a) H_2-TPR profiles of calcined catalysts; (b)XPS spectra of Cu *2p*.

increases, initially there is an increase followed by a decrease in the $Cu^{+}/(Cu^{0}+Cu^{+})$ ratio, with the order being Cu-2In/SiO_2 < Cu/SiO_2 < Cu-0.25In/SiO_2 < Cu-1In/SiO_2 < Cu-0.5In/SiO_2. Similar to the changes observed in BET results, the $Cu^{+}/(Cu^{0}+Cu^{+})$ ratio in Cu-*x*In/SiO_2 (*x* = 0, 0.25, 0.50, 1.0, and 2.0 wt%) catalysts exhibited only minor variations. Therefore, it is challenging to consider it as the primary factor responsible for enhancing the catalyst's adsorption capacity for reactants, this aspect was further validated in subsequent HPM-TPD-MS experiments.

In *3d*-XPS spectra were recorded and deconvoluted of Cu-*x*In/SiO_2 and 2In/SiO_2 after reduction (578 K), as shown in Fig. 5a and Fig. S3. The peak binding energies of 2In/SiO_2 samples are approximately 445.4 eV and 453.0 eV, corresponding to In^{3+} *3d 5/2* and In^{3+} *3d 3/2*, respectively. This suggests that indium remains in the form of oxides within the reduced samples [38,64]. Upon reduction, the In^{3+} *3d* peak of Cu-*x*In/SiO_2 exhibits an asymmetric morphology and undergoes a pronounced blue shift in comparison to the 2In/SiO_2 sample. This observation further indicates an interaction between Cu species and indium species, resulting in electron cloud displacement from the vicinity of In species towards Cu species. The In *3d 5/2* signal in the Cu-*x*In/SiO_2 catalysts were deconvoluted into the contributions of two species—metallic In^{0} and In^{3+}—at 444.6 eV and 446.0 eV [65–68], respectively (Table S3), indicating that a portion of the indium species was reduced to its metallic form under the reduction conditions at 578 K [38,64]. This observation is consistent with the findings from the H_2-TPR analysis. The percentage of In species presented in the form of In^{0} in the fresh catalysts decreases in the order Cu-1In/SiO_2 (19.7 %) > Cu-2In/SiO_2 (16.2 %) > Cu-0.5In/SiO_2 (15.1 %) > Cu-0.25In/SiO_2 (12.3 %). The dispersion of In_2O_3 on a silica support is generally challenging [69], and the reduction behavior of indium is highly dependent on particle size. Smaller grains can be reduced below 578 K, while larger grains require significantly higher temperatures for reduction [70,71]. And the intimate contact between copper and indium species promotes the transfer of hydrogen from Cu to In, thereby facilitating the more facile reduction of indium oxide [72]. This further proved that the adopted preparation method in this study is demonstrated to effectively disperse indium species on the catalyst, facilitating the predominant reduction of indium oxide at 578 K and promoting the formation of CuIn alloy. This further elucidates that the Cu-*x*In/SiO_2 catalyst preparation method employed in this study facilitates the dispersion of In_2O_3 species on the catalyst, thereby enabling partial reduction of indium oxide under the reduction conditions at 578 K and consequently promoting the formation of CuIn alloy.

The correlation between the content ratio (wt%) of In^{0} in the catalyst and its corresponding catalytic activity is illustrated in Fig. 5b. It is observed that the enhancement in conversion rate of the catalyst does not exhibit a linear dependence on the content of CuIn alloy in the catalyst. Therefore, it can be inferred that besides the positive contribution of CuIn alloy, there exist other significant factors contributing to improving hydrogenation activity. The adsorption capacity of catalysts for reactants is a critical determinant of catalytic performance. Consequently, an investigation into the adsorption properties of reactants on the catalysts was undertaken.

3.4. Adsorption ability of the synthesized catalysts for the reactants

To study the adsorption ability of the synthesized catalysts for the reactants, we conducted TPD-MS measurements. The results are shown in Fig. 6a. Specifically, the area of the desorption peak reflects the amount of active species in the catalyst; the desorption temperature correlates with the adsorption strength of the adsorbed reactants on the catalyst [73,74]. A desorption peak for 3-HPM is centered at ca. 500 K for the Cu/SiO_2 catalysts; however, in addition to the desorption peak at low temperature, another desorption band appears at a higher temperature (ca. 570–750 K) for the 2In/SiO_2 and Cu-*x*In/SiO_2 catalysts, suggesting the presence of the multi-status adsorbed 3-HPM. The 2In/SiO_2 catalyst exhibits unexpectedly high adsorption capacity for reactants, likely originating from the presence of highly dispersed In_2O_3 species within the catalyst. The total area for 3-HPM desorption gradually increases in the order Cu/SiO_2 < 2In/SiO_2 < Cu-0.25In/SiO_2 < Cu-0.5In/SiO_2 < Cu-1In/SiO_2 < Cu-2In/SiO_2. Notably, the weakly bound species will then desorb at lower temperatures. Therefore, this observation implies that the incorporation of In species into copper-based catalyst significantly enhances the adsorption capacity for the reactant 3-HPM, thereby facilitating the hydrogenation reaction of 3-HPM.

The correlation between the content ratio (wt%) of In_2O_3 in the catalyst and its corresponding adsorption peak area for 3-HPM is illustrated in Fig. 6b. It can be observed that the adsorption capacity of the catalyst for 3-HPM is closely related to the In_2O_3 content and its dispersion within the catalyst. In general, the modification of copper-based catalyst by introducing highly dispersed In_2O_3 species provided new adsorption sites for reactants, simultaneously enhanced the adsorption capacity for reactants, with the adsorption capacity increasing with the rise in indium content.

Table 3
Summary of data obtained by Cu-XPS and Cu-LMM.

Catalysts	Kinetic energy (eV)		X_{Cu+} (%)	X_{Cu0} (%)	X_{In0} (%)
	Cu^{+}	Cu^{0}			
Cu/SiO_2	913.8	917.5	41.2	58.8	–
Cu-0.25In/SiO_2	914.3	917.6	41.6	58.4	12.3
Cu-0.5In/SiO_2	914.2	917.8	42.2	57.8	15.1
Cu-1In/SiO_2	914.1	917.8	42.0	58.0	19.7
Cu-2In/SiO_2	913.8	917.5	36.6	63.4	16.2

Note: $X_{Cu+} = Cu^{+}/(Cu^{+}+Cu^{0}) \times 100$ %; $X_{Cu0} = Cu^{0}/(Cu^{+}+Cu^{0}) \times 100$ %; $X_{In0} = In^{0}/(In^{3+}+In^{0}) \times 100$ %.

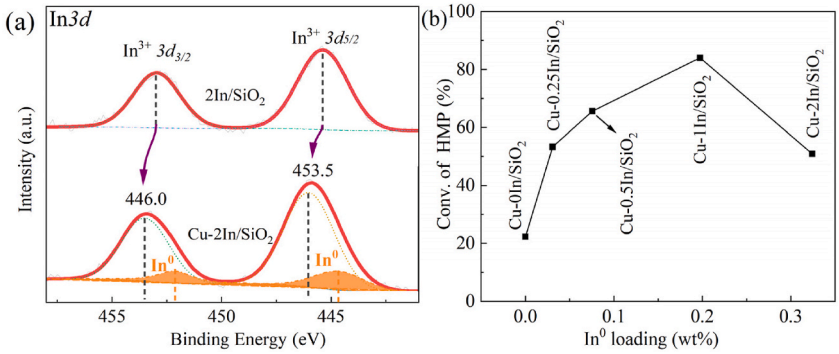

Fig. 5. (a) XPS spectra of In *3d*, (b) the results of the qualitative calculation of the conversion of 3-HPM with In^0 loading (wt%).

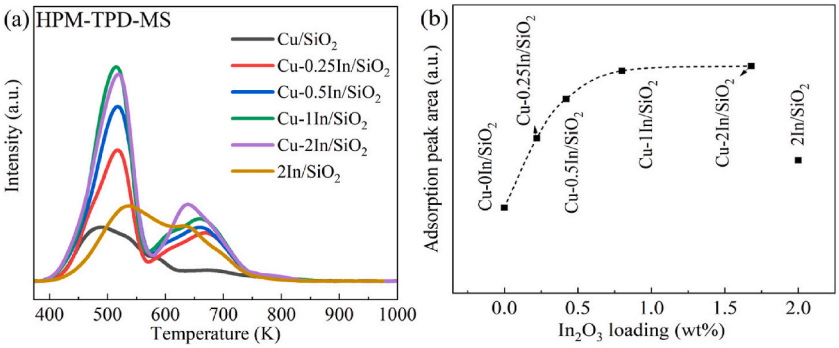

Fig. 6. (a) 3-HPM-TPD-MS profiles of the Cu/SiO_2, $2In/SiO_2$ and Cu-*x*In/SiO_2 catalysts. (b) the results of the qualitative calculation of the adsorption peak area of 3-HPM with In_2O_3 loading (wt%).

3.5. Stability and structure changes of catalysts

The stability of the catalyst was assessed through WHSV(3-HMP) = 0.11 h^{-1}, and the corresponding results are illustrated in Fig. 7. Consequently, the hydrogenation reaction over the Cu-1%In/SiO_2 catalyst at 413K achieved a remarkable conversion of 99.3 % for 3-HPM with a selectivity of 92.2 % towards 1,3-PDO. Notably, the yield of 1,3-PDO obtained using Cu-1%In/SiO_2 reached an impressive 91.5 %, surpassing the yield of Cu/SiO_2 catalyst (264 %) under identical reaction conditions. The catalyst exhibited stable hydrogenation activity during the reaction test for 160 h, followed by a gradual decrease in conversion of 3-HPM (99 %–96 %). Subsequent characterization of the deactivated catalyst was conducted to investigate the factors contributing to its deactivation and provide guidance for future catalyst modification endeavors.

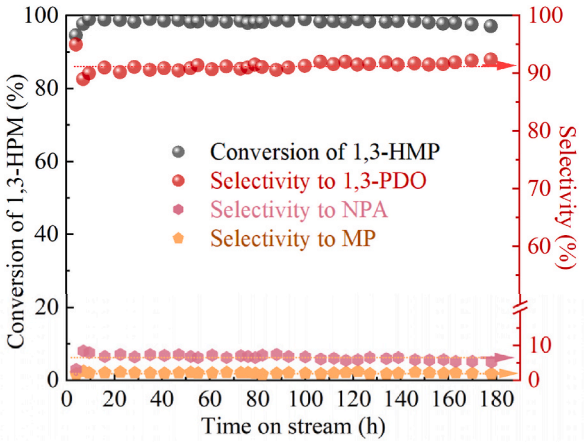

Fig. 7. Stability test of Cu-1In/SiO_2 catalyst. Reaction conditions: T = 413 K, $P(H_2)$ = 6.0 MPa, WHSV(3-HMP) = 0.11 h^{-1}, H_2/3-HPM = 240.

Typically, the deactivation of supported catalysts can be attributed to three primary factors: 1) agglomeration of metal components, 2) loss of active components, and 3) catalyst surface coverage resulting from carbon deposition [6,75–78]. Consequently, the subsequent sections primarily delve into these three aspects to elucidate the mechanisms underlying Cu-1In/SiO_2 catalyst deactivation. The metal particle size in the catalyst gradually increased from 2.6 nm to 4.8 nm before and after the reaction (Fig. S4), with no significant increase observed in the Cu^0 and Cu_2O diffraction peaks in XRD analysis (Fig. S5). This indicates that, during the catalytic hydrogenation reaction, there is minor agglomeration of Cu components, suggesting that the partial cause of catalyst deactivation is the agglomeration of the metal components. In the ICP-OES analysis of the catalyst before and after the reaction, the concentrations of copper and indium species remained relatively stable (Table S5). Moreover, XPS-XAES testing conducted prior to and following the reaction revealed negligible alterations in Cu^+/Cu^0 ratios (Fig. S6). These findings suggest that no detectable loss of active components occurred during the catalytic hydrogenation process. The TG and DTG curves of the catalysts enabled a quantitative evaluation of coking deposition during the reaction. As depicted in Fig. S7, distinct changes in weight loss patterns were observed for the catalysts before and after the reaction, occurring at approximately ca. 360–450 K and ca. 450–550 K. The initial segment of disparity arises from chemical adsorption of reactants and products, while the subsequent significant weight loss is attributed to coke deposition. The enhanced coke deposition on the utilized Cu-1In/SiO_2 catalyst, resulting in an additional 8 % decrease in weight compared to the pristine Cu-1In/SiO_2 catalyst, may comprise oligomers formed on the catalyst surface due to unreacted HPM, products and by-products that were not promptly desorbed. The attachment of oligomers to the catalyst surface also significantly impacts the specific surface area and pore structure of the catalyst (Table S5), resulting in an 11.3 % decrease in S_{BET} and a 19.2 % decrease in V_p. This observation suggests that the presence of oligomers on the catalyst surface, leading to metal coverage and modifications to the structural integrity of the catalyst, constitutes one of the crucial factors contributing to the decline in catalytic activity. Overall, the main reasons for the decline in catalyst activity during the reaction time are primarily attributed to the blockage of catalyst pore structures and masking of catalytic active sites by carbon deposition generated during the catalytic process. Another contributing factor is the partial aggregation of copper nanoparticles.

4. Conclusions

A series of Cu-*x*In/SiO_2 catalysts were synthesized by Et-AE method for the hydrogenation of 3-HPM to 1,3-PDO at low temperatures, and the effects of indium species introduction on the catalytic behavior of the resultant catalysts were also studied in detail. Compared with the catalyst of Cu/SiO_2 prepared, the Cu-1In/SiO_2 catalyst exhibited a superior low temperature catalytic activity in the hydrogenation of 3-HPM to 1,3-PDO, and realized the effective synthesis of 1,3-PDO with a high yield of 91.5 % at the temperature as low as 413 K, which was the lowest temperature for the hydrogenation of 3-HPM to 1,3-PDO in literature. The catalyst exhibited stable hydrogenation activity during the reaction test for 160 h. The characterization results from BET, FT-IR, TG, XRD, TEM, TPR, XPS, XAES, TPD-MS, and ICP-AES indicate that the outstanding catalytic performance of the Cu-In/SiO_2 catalyst primarily arises from two aspects: the interaction between Cu and In, which results in more dispersed copper within the catalyst, and the new reactant adsorption sites introduced by indium oxide. Furthermore, the formation of Cu-In alloy further improves the stability of Cu nanoparticles, maintaining their highly dispersed state, which positively contributes to the overall stability of the catalyst. Fortunately, the introduction of indium species into the catalyst adds new adsorption sites for reactants, enhancing the catalyst's adsorption capacity for reactants. Additionally, the current study investigated potential catalyst deactivation mechanisms, proposing that carbon deposition and metal nanoparticle aggregation are the primary factors contributing to the decline in catalyst activity. In summary, the indium species modification would provide an effective strategy for the Cu-based catalyst synthesis and the as-synthesized Cu-*x*In/SiO_2 exhibit good catalytic activity for the hydrogenation of 3-HPM to 1,3-PDO.

CRediT authorship contribution statement

Chuanming Zhang: Writing – review & editing, Writing – original draft, Data curation, Conceptualization. **Jincan Kang:** Resources, Formal analysis. **Wen Dai:** Writing – review & editing. **Yanbo Peng:** Investigation. **Yiling Zhao:** Methodology. **Xiaoang Yang:** Resources. **Bingni Liu:** Resources. **Hongping Zhu:** Resources, Funding acquisition.

Data availability statement

The authors confirm that the data supporting the findings of this study are available within the article. For additional information or specific requests related to the data, please contact the corresponding author.

Declaration of competing interest

The authors declare that they have no known competing financial interests or personal relationships that could have appeared to influence the work reported in this paper.

Acknowledgements

The National Natural Science Foundation of China (22225104, 22372136, and 21972112), Researching Foundation of Fujian Province (201H6002) and China Postdoctoral Science Foundation (Nos. 2022TQ0115 and 2022M711297) is acknowledged for the

financial support.

Appendix A. Supplementary data

Supplementary data to this article can be found online at https://doi.org/10.1016/j.heliyon.2024.e39723.

References

[1] W. Liu, A.K. Mohanty, L.T. Drzal, M. Misra, J.V. Kurian, R.W. Miller, N. Strickland, Injection molded glass fiber reinforced poly(trimethylene terephthalate) composites: fabrication and properties evaluation, Ind. Eng. Chem. Res. 44 (2005) 857–862.
[2] J.V. Kurian, A new polymer platform for the future — sorona® from corn derived 1,3-propanediol, J. Polym. Environ. 13 (2005) 159–167.
[3] G.A. Kraus, Synthetic methods for the preparation of 1,3-propanediol, clean: soil, Air, Water 36 (2008) 648–651.
[4] Z. Yu, Y. Jie, W. Gongying, Progress in the synthesis of 1, 3-propanediol, Nat. Gas. Chem. Ind. 31 (2006) 66–74.
[5] Y. Ying, K. Feng, Z. Lv, J. Gao, Study on nanon copper-based catalysts for the hydrogenation of methyl 3-hydroxypropionate to 1,3-propanediol, Surf. Rev. Lett. 16 (2009) 343–349.
[6] R.-P. Ye, L. Lin, L.-C. Wang, D. Ding, Z. Zhou, P. Pan, Z. Xu, J. Liu, H. Adidharma, M. Radosz, M. Fan, Y.-G. Yao, Perspectives on the active sites and catalyst design for the hydrogenation of dimethyl oxalate, ACS Catal. 10 (2020) 4465–4490.
[7] E.Y. Lai, Y.T. Zhou, W.J. Li, L.L. Lin, Y.L. Chen, C.M. Zhang, H.P. Zhu, Thermodynamic calculation of the synthesis of 1,3-propanediol by hydrogenation of methyl 3-hydroxypropionate, J. Xiamen Univ. Nat. Sci 62 (2023) 31–38.
[8] S. Zhu, X. Gao, Y. Zhu, W. Fan, J. Wang, Y. Li, A highly efficient and robust Cu/SiO_2 catalyst prepared by the ammonia evaporation hydrothermal method for glycerol hydrogenolysis to 1,2-propanediol, Catal. Sci. Technol. 5 (2015) 1169–1180.
[9] Y. Zhao, S. Li, Y. Wang, B. Shan, J. Zhang, S. Wang, X. Ma, Efficient tuning of surface copper species of Cu/SiO_2 catalyst for hydrogenation of dimethyl oxalate to ethylene glycol, Chem. Eng. J. 313 (2017) 759–768.
[10] D.S. Brands, E.K. Poels, A. Bliek, Ester hydrogenolysis over promoted Cu/SiO_2 catalysts, Appl. Catal., A 184 (1999) 279–289.
[11] H. Guzman, D. Roldan, A. Sacco, M. Castellino, M. Fontana, N. Russo, S. Hernandez, CuZnAl-oxide nanopyramidal mesoporous materials for the electrocatalytic CO_2 reduction to syngas: tuning of H_2/CO ratio, Nano 11 (2021) 1–27.
[12] E.K. Poels, D.S. Brands, Modification of Cu/ZnO/SiO_2 catalysts by high temperature reduction, Appl. Catal., A 191 (1999) 83–96.
[13] M.A.N. Santiago, M.A. Sánchez-Castillo, R.D. Cortright, J.A. Dumesic, Catalytic reduction of acetic acid, methyl acetate, and ethyl acetate over silica-supported copper, J. Catal. 193 (2000) 16–28.
[14] A. Yin, C. Wen, W.-L. Dai, K. Fan, Nanocasting of CuAu alloy nanoparticles for methyl glycolate synthesis, J. Mater. Chem. 21 (2011) 8997–8999.
[15] Y.-n. Wang, X. Duan, J. Zheng, H. Lin, Y. Yuan, H. Ariga, S. Takakusagi, K. Asakura, Remarkable enhancement of Cu catalyst activity in hydrogenation of dimethyl oxalate to ethylene glycol using gold, Catal. Sci. Technol. 2 (2012) 1637–1639.
[16] B. Wang, Q. Xu, H. Song, G. Xu, Synthesis of methyl glycolate by hydrogenation of dimethyl oxalate over Cu-Ag/SiO_2 catalyst, J. Nat. Gas Chem. 16 (2007) 78–80.
[17] Y. Liu, J. Ding, J. Yang, J. Bi, K. Liu, J. Chen, Stabilization of copper catalysts for hydrogenation of dimethyl oxalate by deposition of Ag clusters on Cu nanoparticles, Catal. Commun. 98 (2017) 43–46.
[18] A. Yin, C. Wen, X. Guo, W.-L. Dai, K. Fan, Influence of Ni species on the structural evolution of Cu/SiO_2 catalyst for the chemoselective hydrogenation of dimethyl oxalate, J. Catal. 280 (2011) 77–88.
[19] B. Xiong, Y. Yang, J. Liu, J. Ding, Y. Yang, Electrochemical conversion of CO_2 to syngas over Cu-M (M = Cd, Zn, Ni, Ag, and Pd) bimetal catalysts, Fuel 304 (2021) 121341–121348.
[20] P. Ai, M. Tan, P. Reubroycharoen, Y. Wang, X. Feng, G. Liu, G. Yang, N. Tsubaki, Probing the promotional roles of cerium in the structure and performance of Cu/SiO_2 catalysts for ethanol production, Catal. Sci. Technol. 8 (2018) 6441–6451.
[21] C.-C. Chen, L. Lin, R.-P. Ye, L. Huang, L.-B. Zhu, Y.-Y. Huang, Y.-Y. Qin, Y.-G. Yao, Construction of Cu-Ce composite oxides by simultaneous ammonia evaporation method to enhance catalytic performance of Ce-Cu/SiO_2 catalysts for dimethyl oxalate hydrogenation, Fuel 290 (2021) 120083–120094.
[22] Y. Zhang, C. Ye, C. Guo, C. Gan, X. Tong, In_2O_3-modified Cu/SiO_2 as an active and stable catalyst for the hydrogenation of methyl acetate to ethanol, Chin. J. Catal. 39 (2018) 99–108.
[23] Y. Xu, L. Kong, H. Huang, H. Wang, X. Wang, S. Wang, Y. Zhao, X. Ma, Promotional effect of indium on Cu/SiO_2 catalysts for the hydrogenation of dimethyl oxalate to ethylene glycol, Catal. Sci. Technol. 11 (2021) 6854–6865.
[24] M.M. Li, J. Zheng, J. Qu, F. Liao, E. Raine, W.C. Kuo, S.S. Su, P. Po, Y. Yuan, S.C. Tsang, The remarkable activity and stability of a highly dispersive beta-brass Cu-Zn catalyst for the production of ethylene glycol, Sci. Rep. 6 (2016) 20527–20535.
[25] S. Kattel, P.J. Ramírez, J.G. Chen, J.A. Rodriguez, P. Liu, Active sites for CO_2 hydrogenation to methanol on Cu/ZnO catalysts, Science 355 (2017) 1296–1299.
[26] X. Wang, M. Chen, X. Chen, R. Lin, H. Zhu, C. Huang, W. Yang, Y. Tan, S. Wang, Z. Du, Y. Ding, Constructing copper-zinc interface for selective hydrogenation of dimethyl oxalate, J. Catal. 383 (2020) 254–263.
[27] M. Behrens, F. Studt, I. Kasatkin, S. Kuhl, M. Havecker, F. Abild-Pedersen, S. Zander, F. Girgsdies, P. Kurr, B.L. Kniep, M. Tovar, R.W. Fischer, J.K. Norskov, R. Schlogl, The active site of methanol synthesis over Cu/ZnO/Al_2O_3 industrial catalysts, Science 336 (2012) 893–897.
[28] W. Qi, Q. Ling, D. Ding, C. Yazhong, S. Chengwu, C. Peng, W. Ye, Z. Qinghong, L. Rong, S. Hao, Performance enhancement of Cu/SiO_2 catalyst for hydrogenation of dimethyl oxalate to ethylene glycol through zinc incorporation, Catal. Commun. 108 (2018) 68–72.
[29] K. Sun, Z. Fan, J. Ye, J. Yan, Q. Ge, Y. Li, W. He, W. Yang, C.-j. Liu, Hydrogenation of CO_2 to methanol over In_2O_3 catalyst, J. CO_2 Util. 12 (2015) 1–6.
[30] L. Wang, Y. Dong, T. Yan, Z. Hu, F.M. Ali, D.M. Meira, P.N. Duchesne, J.Y.Y. Loh, C. Qiu, E.E. Storey, Y. Xu, W. Sun, M. Ghoussoub, N.P. Kherani, A.S. Helmy, G. A. Ozin, Black indium oxide a photothermal CO_2 hydrogenation catalyst, Nat. Commun. 11 (2020) 2432–2440.
[31] O. Martin, A.J. Martin, C. Mondelli, S. Mitchell, T.F. Segawa, R. Hauert, C. Drouilly, D. Curulla-Ferre, J. Perez-Ramirez, Indium oxide as a superior catalyst for methanol synthesis by CO_2 hydrogenation, Angew Chem. Int. Ed. Engl. 55 (2016) 6261–6265.
[32] N. Rui, Z. Wang, K. Sun, J. Ye, Q. Ge, C.-j. Liu, CO_2 hydrogenation to methanol over Pd/In_2O_3: effects of Pd and oxygen vacancy, Appl. Catal., B 218 (2017) 488–497.
[33] M.S. Frei, C. Mondelli, R. García-Muelas, K.S. Kley, B. Puértolas, N. López, O.V. Safonova, J.A. Stewart, D. Curulla Ferré, J. Pérez-Ramírez, Atomic-scale engineering of indium oxide promotion by palladium for methanol production via CO_2 hydrogenation, Nat. Commun. 10 (2019) 3377–3388.
[34] N. Rui, F. Zhang, K. Sun, Z. Liu, W. Xu, E. Stavitski, S.D. Senanayake, J.A. Rodriguez, C.-J. Liu, Hydrogenation of CO_2 to methanol on a $au^{\delta+}$–in_2O_{3-x} catalyst, ACS Catal. 10 (2020) 11307–11317.
[35] M. Li, T.H. My Pham, Y. Ko, K. Zhao, L. Zhong, W. Luo, A. Züttel, Support-dependent Cu–in bimetallic catalysts for tailoring the activity of reverse water gas shift reaction, ACS Sustainable Chem. Eng. 10 (2022) 1524–1535.
[36] Z. Shi, Q. Tan, C. Tian, Y. Pan, X. Sun, J. Zhang, D. Wu, CO_2 hydrogenation to methanol over Cu-In intermetallic catalysts: effect of reduction temperature, J. Catal. 379 (2019) 78–89.
[37] J.L. Snider, V. Streibel, M.A. Hubert, T.S. Choksi, E. Valle, D.C. Upham, J. Schumann, M.S. Duyar, A. Gallo, F. Abild-Pedersen, T.F. Jaramillo, Revealing the synergy between oxide and alloy phases on the performance of bimetallic in–Pd catalysts for CO_2 hydrogenation to methanol, ACS Catal. 9 (2019) 3399–3412.

[38] Z. Shi, M. Pan, X. Wei, D. Wu, Cu-In intermetallic compounds as highly active catalysts for CH_3OH formation from CO_2 hydrogenation, Int. J. Energy Res. 46 (2021) 1285–1298.
[39] C.Y. Regalado Vera, N. Manavi, Z. Zhou, L.-C. Wang, W. Diao, S. Karakalos, B. Liu, K.J. Stowers, M. Zhou, H. Luo, D. Ding, Mechanistic understanding of support effect on the activity and selectivity of indium oxide catalysts for CO_2 hydrogenation, Chem. Eng. J. 426 (2021) 131767–131779.
[40] X. Yu, T.A. Vest, N. Gleason-Boure, S.G. Karakalos, G.L. Tate, M. Burkholder, J.R. Monnier, C.T. Williams, Enhanced hydrogenation of dimethyl oxalate to ethylene glycol over indium promoted Cu/SiO_2, J. Catal. 380 (2019) 289–296.
[41] F. Bossola, T. Roongcharoen, M. Coduri, C. Evangelisti, F. Somodi, L. Sementa, A. Fortunelli, V. Dal Santo, Discovering indium as hydrogen production booster for a Cu/SiO_2 catalyst in steam reforming of methanol, Appl. Catal., B 297 (2021) 120398–120411.
[42] H.P. Zhu, J.B. Zhao, Q. Chen, R. Liu, M.Y. He, J.F. Qian, S.Y. Xie, Nitrogen-phosphorus Coordination Metal Catalyst and Method for Preparation of Methyl 3-hydroxypropionate, in, China, 2019.
[43] Q. Hu, G. Fan, S. Zhang, L. Yang, F. Li, Gas phase hydrogenation of dimethyl-1,4-cyclohexane dicarboxylate over highly dispersed and stable supported copper-based catalysts, J. Mol. Catal. Chem. 397 (2015) 134–141.
[44] K.S.W. Sing, D.H. Everett, R.A.W. Haul, L. Moscou, R.A. Pierotti, J. Rouquérol, T. Siemieniewska, Reporting physisorption data for gas/solid systems, Pure Appl. Chem. 57 (1985) 603–619.
[45] C.J.G.V.D. Grift, P.A. Elberse, A. Mulder, J.W. Geus, Preparation of silica-supported copper catalysts by means of deposition-precipitation, Appl. Catal., A 59 (1990) 275–289.
[46] L. Chen, P. Guo, M. Qiao, S. Yan, H. Li, W. Shen, H. Xu, K. Fan, Cu/SiO_2 catalysts prepared by the ammonia-evaporation method: texture, structure, and catalytic performance in hydrogenation of dimethyl oxalate to ethylene glycol, J. Catal. 257 (2008) 172–180.
[47] C.-C. Chen, L. Lin, R.-P. Ye, M.-L. Sun, J.-X. Yang, F. Li, Y.-G. Yao, Mannitol as a novel dopant for Cu/SiO_2: a low-cost, environmental and highly stable catalyst for dimethyl oxalate hydrogenation without hydrogen prereduction, J. Catal. 389 (2020) 421–431.
[48] J. Yu, J. Cao, L. Du, Y. Wei, T. Wang, H. Tian, Enhancement of diethyl malonate hydrogenation to 1,3-propanediol using mesoporous Cu/SBA-15 as catalyst, Appl. Catal., A 555 (2018) 161–170.
[49] Z. He, H. Lin, P. He, Y. Yuan, Effect of boric oxide doping on the stability and activity of a $Cu–SiO_2$ catalyst for vapor-phase hydrogenation of dimethyl oxalate to ethylene glycol, J. Catal. 277 (2011) 54–63.
[50] T. Toupance, M. Kermarec, J.-F. Lambert, C. Louis, Conditions of formation of copper phyllosilicates in silica-supported copper catalysts prepared by selective adsorption, J. Phys. Chem. B 106 (2002) 2277–2286.
[51] X. Zheng, H. Lin, J. Zheng, X. Duan, Y. Yuan, Lanthanum oxide-modified Cu/SiO_2 as a high-performance catalyst for chemoselective hydrogenation of dimethyl oxalate to ethylene glycol, ACS Catal. 3 (2013) 2738–2749.
[52] X. Dong, X. Ma, H. Xu, Q. Ge, Comparative study of silica-supported copper catalysts prepared by different methods: formation and transition of copper phyllosilicate, Catal. Sci. Technol. 6 (2016) 4151–4158.
[53] Z. Ma, Z. Xiao, J.A. van Bokhoven, C. Liang, A non-alkoxide sol–gel route to highly active and selective Cu–Cr catalysts for glycerol conversion, J. Mater. Chem. 20 (2010) 755–760.
[54] S. Rasul, D.H. Anjum, A. Jedidi, Y. Minenkov, L. Cavallo, K. Takanabe, A highly selective copper-indium bimetallic electrocatalyst for the electrochemical reduction of aqueous CO_2 to CO, Angew Chem. Int. Ed. Engl. 54 (2015) 2146–2150.
[55] S. Zhao, H. Yue, Y. Zhao, B. Wang, Y. Geng, J. Lv, S. Wang, J. Gong, X. Ma, Chemoselective synthesis of ethanol via hydrogenation of dimethyl oxalate on Cu/SiO_2 : enhanced stability with boron dopant, J. Catal. 297 (2013) 142–150.
[56] X. Kong, C. Ma, J. Zhang, J. Sun, J. Chen, K. Liu, Effect of leaching temperature on structure and performance of Raney Cu catalysts for hydrogenation of dimethyl oxalate, Appl. Catal., A 509 (2016) 153–160.
[57] A. Yin, X. Guo, K. Fan, W.-L. Dai, Influence of copper precursors on the structure evolution and catalytic performance of Cu/HMS catalysts in the hydrogenation of dimethyl oxalate to ethylene glycol, Appl. Catal., A 377 (2010) 128–133.
[58] Y. Zhao, H. Zhang, Y. Xu, S. Wang, Y. Xu, S. Wang, X. Ma, Interface tuning of Cu^+/Cu^0 by zirconia for dimethyl oxalate hydrogenation to ethylene glycol over Cu/SiO_2 catalyst, J. Energy Chem. 49 (2020) 248–256.
[59] C. Xu, G. Chen, Y. Zhao, P. Liu, X. Duan, L. Gu, G. Fu, Y. Yuan, N. Zheng, Interfacing with silica boosts the catalysis of copper, Nat. Commun. 9 (2018) 3366–3375.
[60] H. Lin, X. Zheng, Z. He, J. Zheng, X. Duan, Y. Yuan, Cu/SiO_2 hybrid catalysts containing HZSM-5 with enhanced activity and stability for selective hydrogenation of dimethyl oxalate to ethylene glycol, Appl. Catal., A 445–446 (2012) 287–296.
[61] X. Ma, H. Chi, H. Yue, Y. Zhao, Y. Xu, J. Lv, S. Wang, J. Gong, Hydrogenation of dimethyl oxalate to ethylene glycol over mesoporous Cu-MCM-41 catalysts, AIChE J. 59 (2013) 2530–2539.
[62] C. Wen, A. Yin, Y. Cui, X. Yang, W.-L. Dai, K. Fan, Enhanced catalytic performance for $SiO_2–TiO_2$ binary oxide supported Cu-based catalyst in the hydrogenation of dimethyloxalate, Appl. Catal., A 458 (2013) 82–89.
[63] Y. Zhu, Y. Zhu, G. Ding, S. Zhu, H. Zheng, Y. Li, Highly selective synthesis of ethylene glycol and ethanol via hydrogenation of dimethyl oxalate on Cu catalysts: influence of support, Appl. Catal., A 468 (2013) 296–304.
[64] G. Chen, L. Wang, X. Sheng, L. Chang, Y. Luo, D. Yang, Structural characterization of $CuInS_2$ thin films from Cu–In metal inks, Phys. Status Solidi A 208 (2011) 2399–2405.
[65] G.O. Larrazábal, A.J. Martín, S. Mitchell, R. Hauert, J. Pérez-Ramírez, Enhanced reduction of CO_2 to CO over Cu–in electrocatalysts: catalyst evolution is the key, ACS Catal. 6 (2016) 6265–6274.
[66] T. Sivaranjani, T.A. Revathy, S. Dhanavel, K. Dhanapal, V. Narayanan, A. Stephen, Effect of dendritic Cu-in alloy on Cr(VI) reduction synthesized via pulsed electrodeposition, ChemistrySelect 3 (2018) 12613–12619.
[67] P. Sen, M.S. Hegde, C.N.R. Rao, Surface oxidation of cadmium, indium, tin and antimony by photoelectron and Auger spectroscopy, Appl. Surf. Sci. 10 (1982) 63–74.
[68] A.W.C. Lin, N.R. Armstrong, T. Kuwana, X-ray photoelectron/Auger electron spectroscopic studies of tin and indium metal foils and oxides, Anal. Chem. 49 (1977) 668A–757A.
[69] A. Gervasini, J.A. Perdigon-Melon, C. Guimon, A. Auroux, An in-depth study of supported In_2O_3 catalysts for the selective catalytic reduction of NO_x: the influence of the oxide support, J. Phys. Chem. B 110 (2006) 240–249.
[70] P.W. Park, C.S. Ragle, C.L. Boyer, M.L. Balmer, M. Engelhard, D. McCready, In_2O_3/Al_2O_3 catalysts for NO_x reduction in lean condition, J. Catal. 210 (2002) 97–105.
[71] M. Chen, J. Xu, Y. Cao, H.-Y. He, K.-N. Fan, J.-H. Zhuang, Dehydrogenation of propane over $In_2O_3–Al_2O_3$ mixed oxide in the presence of carbon dioxide, J. Catal. 272 (2010) 101–108.
[72] X. Dong, J. Lei, Y. Chen, H. Jiang, M. Zhang, Selective hydrogenation of acetic acid to ethanol on Cu-In catalyst supported by SBA-15, Appl. Catal. B Environ. 244 (2019) 448–458.
[73] X.Y. Li, Y. Wang, L.H. Kang, M.Y. Zhu, B. Dai, A novel, non metallic graphitic carbon nitride catalyst for acetylene hydrochlorination, J. Catal. 311 (2014) 288–294.
[74] C.F. Huang, M.Y. Zhu, L.H. Kang, X.Y. Li, B. Dai, Active carbon supported $TiO_2–AuCl_3$/AC catalyst with excellent stability for acetylene hydrochlorination reaction, Chem. Eng. J. 242 (2014) 69–75.
[75] M.B. Gawande, A. Goswami, F.X. Felpin, T. Asefa, X. Huang, R. Silva, X. Zou, R. Zboril, R.S. Varma, Cu and Cu-based nanoparticles: synthesis and applications in catalysis, Chem. Rev. 116 (2016) 3722–3811.

[76] Z. Wang, Z. Xu, S. Peng, Z. Zhou, P. Pan, L. Lin, Y. Qin, G. Guo, Y. Yao, New catalysts for coal to ethylene glycol, Chin. J. Chem. 35 (2017) 759–768.
[77] R.-P. Ye, L. Lin, Q. Li, Z. Zhou, T. Wang, C.K. Russell, H. Adidharma, Z. Xu, Y.-G. Yao, M. Fan, Recent progress in improving the stability of copper-based catalysts for hydrogenation of carbon–oxygen bonds, Catal. Sci. Technol. 8 (2018) 3428–3449.
[78] J. Niu, H. Liu, Y. Jin, B. Fan, W. Qi, J. Ran, Comprehensive review of Cu-based CO_2 hydrogenation to CH_3OH: insights from experimental work and theoretical analysis, Int. J. Hydrogen Energy 47 (2022) 9183–9200.